A&A 516, A74 (2010)
DOI: 10.1051/0004-6361/201014361

Astronomy & Astrophysics

Thermal properties of asteroid 21 Lutetia from *Spitzer* Space Telescope observations

P. L. Lamy[1], O. Groussin[1], S. Fornasier[2,3], L. Jorda[1], M. Kaasalainen[4], and M. A. Barucci[2]

[1] Laboratoire d'Astrophysique de Marseille, UMR6110 CNRS/Université de Provence, 38 rue Frédéric Joliot-Curie, 13388 Marseille Cedex 13, France
e-mail: philippe.lamy@oamp.fr
[2] LESIA, Observatoire de Paris, 92195 Meudon Principal Cedex, France
[3] Université de Paris 7 Denis Diderot, France
[4] Tampere University of Technology, Finland

Received 5 March 2010 / Accepted 7 May 2010

ABSTRACT

Context. Asteroid 21 Lutetia is the second target of the Rosetta space mission with a flyby scheduled in July 2010. To best prepare the observational campaign, Lutetia is being extensively characterized by ground- and space-based astronomical facilities.
Aims. We used the *Spitzer* Space Telescope (SST) to determine the thermal properties of Lutetia and more generally, to contrain its physical properties and nature.
Methods. The observations were performed with the infrared spectrograph (IRS) of the SST on 10 and 11 December 2005, when the asteroid was 2.81 AU from the Sun, 2.65 AU from the SST and at a phase angle of 21°. We obtained 14 spectra ranging from 5.2 to 38.0 μm, and sampling the rotational period of the asteroid. They were interpreted with a standard thermal model incorporating the thermal inertia.
Results. We obtained the first thermal light curve of Lutetia. Using the most recent solution for its three-dimensional shape and rotational state, as well as independently determined parameters such as the albedo, we satisfactorily reproduced the 14 spectral energy distributions and the complete thermal light curve of Lutetia. The best thermal model has a thermal inertia $I \leq 30$ JK^{-1}m^{-2}s$^{-1/2}$ and a beaming factor in the range ~0.70–0.83. This low thermal inertia is typical of main belt asteroids and implies that the surface of Lutetia is likely covered by a thick regolith layer. Since the beaming factor only reflects the effects of surface rugosity, the above range implies a high degree of roughness. In addition, our results show evidence of inhomogeneities in the surface roughness in the equatorial band of Lutetia.

Key words. minor planets, asteroids: general – minor planets, asteroids: individual: 21 Lutetia – techniques: image processing

1. Introduction

The Rosetta spacecraft was successfully launched on 2 March 2004 and is now on its way to rendezvous with comet 67P/Churyumov-Gerasimenko in May 2014 at a heliocentric distance of 4.5 AU. During its journey to the comet, the spacecraft has already flown by asteroid 2867 Steins on 5 September 2008 at a velocity of 8.6 km/s and a closest approach of 803 km (Keller et al. 2010). It will next fly by another main belt asteroid, 21 Lutetia, on 10 July 2010 at a velocity of 15 km s^{-1} and a closest approach of 3055 km. As for all targets of space missions, an a-priori knowledge of these "terra incognita" is crucial for preparing and optimizing the operations of the spacecraft and its instruments so as to maximize the scientific return. We have already performed a detailed characterization of asteroid 2867 Steins before its flyby, in particular on the basis of extensive thermal observations performed with the *Spitzer* Space Telescope (SST), see Lamy et al. (2008). We now turn our attention to the second target asteroid, 21 Lutetia, and report on the results coming from similar SST observations.

The large main belt asteroid, 21 Lutetia, is about 100 km in diameter. It was first observed in the infrared by the IRAS satellite and the main outcome was a relatively high value for the geometric albedo, $p_V = 0.22 \pm 0.02$ where the V subscript refers to the V photometric band (Tedesco & Veeder 1992) leading to an M-type taxonomic classification and suggesting a metallic composition. Mueller et al. (2006) performed thermal photometry in three, narrow-bandwidth, filters centered at 8.7, 11.6, and 18.4 μm and analyzed their data with a variety of thermal models. They obtained a geometric albedo p_V in the range 0.19 ± 0.06 to 0.235 ± 0.05 depending upon the model being used, a best-fit thermal inertia $I \simeq 50$ JK^{-1}m^{-2}s$^{-1/2}$ (but point out that a thermal inertia of zero was compatible with their data), and a beaming factor $\eta \simeq 0.93$. Altogether, this implies that Lutetia has thermal properties that are fairly typical of main-belt asteroids, i.e., low thermal inertia and some surface roughness. Carvano et al. (2008) performed thermal photometry in three narrow-bandwidth filters centered at 8.7, 10.49, and 12.35 μm and also acquired a (quite noisy) low dispersion N-band spectrum ranging from 8 to 12.5 μm. They analyzed their data with their own thermophysical model, which solves for the thermal balance of the individual facets composing the shape model of the asteroid (i.e., similar to a method we implemented in similar past studies, see for instance Groussin et al. 2004) but also introduce craters to model the rugosity of the surface, each crater being divided into a number of tiles, all this at the expense of additional, unknown parameters. They obtained a geometric albedo $p_V = 0.129$ and a very low thermal inertia of $I \simeq 5$ JK^{-1}m^{-2}s$^{-1/2}$, interpreted as evidence of a well-developed regolith layer with low thermal conductivity, suggestive of high surface microporosity.

Table 1. Observational circumstances for the observations of 21 Lutetia with the SST on 10 and 11 December 2005.

Target [set]	Date	UT_{start} (hh:mm:ss)	UT_{end} (hh:mm:ss)	r (AU)	Δ (AU)	α (°)
Lutetia [01]	10 Dec.	17:32:45	17:36:11	2.8102330	2.6573956	21.12
Lutetia [02]	10 Dec.	18:28:06	18:31:32	2.8102551	2.6568463	21.13
Lutetia [03]	10 Dec.	19:01:37	19:05:03	2.8102661	2.6565717	21.13
Lutetia [04]	10 Dec.	19:44:44	19:48:10	2.8102826	2.6561597	21.13
Lutetia [05]	10 Dec.	20:18:06	20:21:33	2.8102935	2.6558849	21.13
Lutetia [06]	10 Dec.	21:07:53	21:11:19	2.8103101	2.6554730	21.13
Lutetia [07]	10 Dec.	21:37:15	21:40:41	2.8103211	2.6551983	21.13
Lutetia [08]	10 Dec.	22:25:30	22:28:56	2.8103431	2.6546488	21.13
Lutetia [09]	10 Dec.	23:07:46	23:11:13	2.8103540	2.6543741	21.13
Lutetia [10]	10 Dec.	23:40:07	23:43:33	2.8103705	2.6539620	21.13
Lutetia [11]	11 Dec.	00:28:35	00:32:01	2.8103869	2.6535499	21.13
Lutetia [12]	11 Dec.	01:05:54	01:09:20	2.8103979	2.6532752	21.13
Lutetia [13]	11 Dec.	01:41:51	01:45:17	2.8104144	2.6528631	21.13
Lutetia [14]	11 Dec.	02:23:52	02:27:18	2.8104308	2.6524509	21.13

Notes. r_h, Δ: Distances from Lutetia to respectively the Sun and the SST; α: solar phase angle as seen from the SST.

The observed thermal emission of an asteroid is, to a large extent, determined by its shape, size, rotational state, albedo, thermal inertia, and surface roughness. The analysis of the radiometric measurements is seriously hampered, and can even be flawed if knowledge of them is limited or, worse, incorrect if an over-simplified thermal model is used.

Our present analysis benefits from major improvements on two fronts. First, high-angular-resolution, adaptive-optics images were acquired during the 2008 opposition allowing to resolve Lutetia, and to improve the determination of its size, shape, and spin axis (Drummond et al. 2009; Carry et al. 2010; Merline et al., in prep.) compared to the early solution of Torppa et al. (2003). Second, recent photometric observations analyzed with up-to-date shape models (Lamy et al. 2010; Weaver et al. 2010), as well as polarimetric observations (Belskaya et al. 2010), have allowed pinning down the determination of the albedo. Coupled with our unprecedented data set of 14 spectra ranging from 5.2 to 38.0 μm that sample the rotational period of the asteroid and obtained under the ideal conditions of a space observatory, we are in a position to make progress on the question of the thermophysical properties of Lutetia.

The present article is organized as follows. We first present the SST observations of 21 Lutetia, the data reduction, and the set of resulting spectral energy distributions (SEDs). We then introduce the most recent shape model and the thermal model we implemented to analyze the above results, and discuss the parameters. Our results are next presented, and we discuss their implications in terms of the physical properties of the asteroid. We finally produce thermal maps of Lutetia at the time and under the geometric conditions of the Rosetta flyby.

2. Observations with the *Spitzer* space telescope

There were only two visibility windows of about 20 days each to observe 21 Lutetia with the SST during cycle 2 because of the restriction on solar elongation (80–120°). The scheduled window was chosen so as to minimize the thermal flux expected from Lutetia to avoid saturation of the detectors. The observations took place on 10 and 11 December 2005, the asteroid being at a heliocentric distance of 2.81 AU, at a distance from the SST of 2.65 AU, and at a solar phase angle of 21°. The current determination of the direction of the rotational axis of Lutetia implies an aspect angle (defined as the angle between the spin vector and the asteroid-observer vector) of 75°, close to an equatorial view. We used the infrared spectrograph (IRS) in the low-resolution mode ($R = \lambda/\Delta\lambda \sim 64-128$), which covers the wavelength range 5.2–38 μm in four long-slit segments: the short wavelength, 2nd order (SL2, from 5.2 to 8.5 μm); the short wavelength, 1st order (SL1, from 7.4 to 14.2 μm); the long wavelength, 2nd order (LL2, from 14.0 to 21.5 μm); and the long wavelength, 1st order (LL1, from 19.5 to 38.0 μm). The observational sequence was repeated 14 times at time interval of ~40 min from UT 17:32 on 10 December to UT 02:27 on 11 December 2005 in order to fully sample its rotational period of ~8.2 h. The observational circumstances for the observations are reported in Table 1. All spectra were acquired with a single ramp of 6.29 s. The pointing of the target was performed using the ephemeris derived from the Horizon database maintained by the Solar System Dynamics Group at the Jet Propulsion Laboratory. In addition, we used the blue peak-up camera to obtain images at 16 μm, and placed the asteroid image inside the slits with high accuracy. This was indeed required because Lutetia is a moving target and the SL mode has slits that are only 3.6 arcsec wide, while the slits are larger (10.6 arcsec) for the LL mode. Details about the SST and its infrared spectrograph can be found in Werner et al. (2004) and in the *Spitzer* observer's manual (http://ssc.spitzer.caltech.edu/documents/SOM/irs60.pdf).

2.1. Data reduction

The science data coming from the IRS instrument are received and processed at the *Spitzer* Space Center (SSC). We used the basic calibrated data (BCD) produced by an automated data reduction pipeline (version S13.0) that includes cosmic ray removal, dark current subtraction, collapsing cubes to two-dimensional flux images by fitting ramp slopes, flat fielding, and stray light correction. A detailed description of the pipeline reduction steps can be found in Houck et al. (2004) and in the IRS *Spitzer* observer's manual – IRS pipeline handbook (http://ssc.spitzer.caltech.edu/irs/dh/). The calibration dataset was provided by the SSC along with the scientific data.

The sky subtraction is not performed by the automated pipeline. The background of the IRS images is dominated by the zodiacal cloud with a minor component from the interstellar medium. We performed the sky correction by calculating the difference between the two nod positions available for

the observations in each spectral segment, following a standard "chopping" technique usually applied to ground-based infrared observations. The offset (one third of the slit length) is large enough that compact objects have no overlapping pixels in the two dispersed images.

We extracted the one-dimensional spectra in the four IRS segments using SPICE, the *Spitzer* IRS Custom Extraction software in JAVA language (version 1.3). The extraction pipeline takes the two-dimensional, background-subtracted, BCD image in FITS format as input. Each BCD image has an associated uncertainty and bitmask file, which indicates individual pixel status.

The SPICE spectral extraction thread consists of four modules.

1. It creates wavelength-collapsed average spatial profile of the slit used in the observation.
2. The location of the peak in the PROFILE output is identified for the point source extraction.
3. The spectrum is extracted (flux is in electron/s) along the RIDGE location in accordance with the wavelength-dependent point spread function (PSF) and the spectral profile. It must be noted that the source spectrum incident on the array is not rectilinear in either the spectral or cross-dispersed directions. As a result, the EXTRACT module does not extract whole pixels, but instead subdivides the array into a network of polygon-shaped sampling elements referred to as "pseudo-rectangles", which do not necessarily overlap the rectangular pixel grid. These elements allow Nyquist sampling of spectra in the dispersion direction. Extraction is performed by calculating the signal that falls within the boundary of the "pseudo-rectangles". Light is assumed to be evenly distributed within a pixel for purposes of calculating fractional contribution.
4. The software applies photometric tuning and flux conversion coefficients to the 1D spectra, getting a flux in Jy. This module also corrects the slope and curvature of each order by applying polynomial coefficients based on the calibration dataset. This correction is based on an order-by-order comparison of calibration data to standard star model spectra.

2.2. Uncertainties

According to the SPICE data handbook, pointing uncertanties with high-accuracy peak-up will result in photometric uncertainties of ±2% within a given nod position. However mismatches between different low-resolution modules may be as much as 5%. "Jumps" in flux between the SL and LL spectral orders for a source observed with both modules are typically less than 5%, once background emissions from zodiacal dust and cirrus have been removed. The point source calibration is based on an average of multiple observations of the standard star. Due to differences in the fluxes of each nod, an individual observation may show other mismatches between SL and LL.

2.3. Results

The fourteen SEDs over the full spectral range 5–38 μm are displayed in Fig. 1. The fluxes reached the expected level so that the signal-over-noise ratio is excellent, just slightly degraded beyond about 33 μm.

3. Analysis of the thermal data

Interpretation of the infrared data requires both a shape model and a thermal model, which are described below.

3.1. Shape model

High-angular-resolution adaptive-optics (AO) images were acquired at different large telescopes during the 2008 opposition and resolved Lutetia thus leading to improved estimates of its size, shape, and spin axis (Drummond et al. 2009; Carry et al. 2010; Merline et al., in prep.) that supersede the earlier solutions resulting from the inversion by Torppa et al. (2003) of a set of light curves (LC) obtained from 1962 to 1998. Contrary to LC inversion, which gives only a relative shape, the AO images yield the absolute size of the models. The triaxial ellipsoid model derived by Drummond et al. (2009) on the basis of AO images alone has an overall size of $132 \times 101 \times 76$ km and a spin axis direction defined by ecliptic longitude $\lambda = 49°$ and ecliptic latitude $\beta = -8°$. In this study, we use a more elaborated solution that combines AO and LC information, thus producing a more "realistic" shape model. The overall dimensions measured along the principal axes of inertia are $127 \times 107 \times 101$ km, and the spin axis direction is defined by $\lambda = 52°$ and $\beta = -6°$. We used a re-sampled version of the shape model, composed of 1112 triangular facets. Figure 2 displays the 14 views of Lutetia as it would have appeared to the SST in the visible (i.e., reflected light) at the time of the 14 visits.

3.2. Thermal model

The thermal model describes the energy balance on the surface between the flux received from the Sun, the re-radiated flux, and the heat conduction into the asteroid. The surface energy balance for each facet of the shape model with index i is given by Eq. (1):

$$(1 - A_v)\frac{F_{sun}}{r_h^2} v_i \cos(z_i) = \eta\epsilon\sigma T_i^4 + \kappa \left.\frac{\partial T_i}{\partial x}\right|_{x=0} \quad (1)$$

where A_v is the Bond albedo in the V band; F_{sun} [Wm^{-2}] the solar constant; r_h [AU] the heliocentric distance; v_i the illumination factor of facet i ($v_i = 1$ if the facet is illuminated and $v_i = 0$ if the facet is in shadow); z_i the zenithal angle of facet i; η the beaming factor that follows the strict definition given by Lagerros (1998) in the sense that it only reflects the influence of surface roughness; ϵ the infrared emissivity; T_i [K] is the surface temperature of facet i; κ [Wm^{-1}K^{-1}] is the thermal conductivity and x measures the depth. Numerical values for the parameters are discussed below. Our model is very similar to the thermophysical model (TPM) developed by Lagerros (1996, 1998) and only differs in the way it deals with beaming. The TPM is based on a two-parameter beaming representation with f the fraction of the surface covered by craters and ρ the rms value of the surface slopes, while our model is based on a single parameter only (η).

As the asteroid rotates around its spin axis, the values of v_i and z_i change, and the heat equation conduction is computed for each facet. We considered the one-dimensional (x), time-dependent (t) equation for the heat conduction, given by Eq. (2):

$$\rho C \frac{\partial T_i(x,t)}{\partial t} = \frac{\partial}{\partial x}\left(\kappa \frac{\partial T_i(x,t)}{\partial x}\right) \quad (2)$$

where ρ [kg/m^3] is the bulk density, and C [J/kg/K] the specific heat capacity of the asteroid. We solved Eqs. (1) and (2) using a method similar to that of Spencer et al. (1989), and described in Groussin et al. (2004), which involves the thermal inertia $I = \sqrt{\kappa\rho C}$ [JK^{-1}m^{-2}s$^{-1/2}$]. We used a time step of 9 s, which is small enough compared to the rotation period (8.2 h) to insure relaxation of the numerical solution in 30 rotations. As a result,

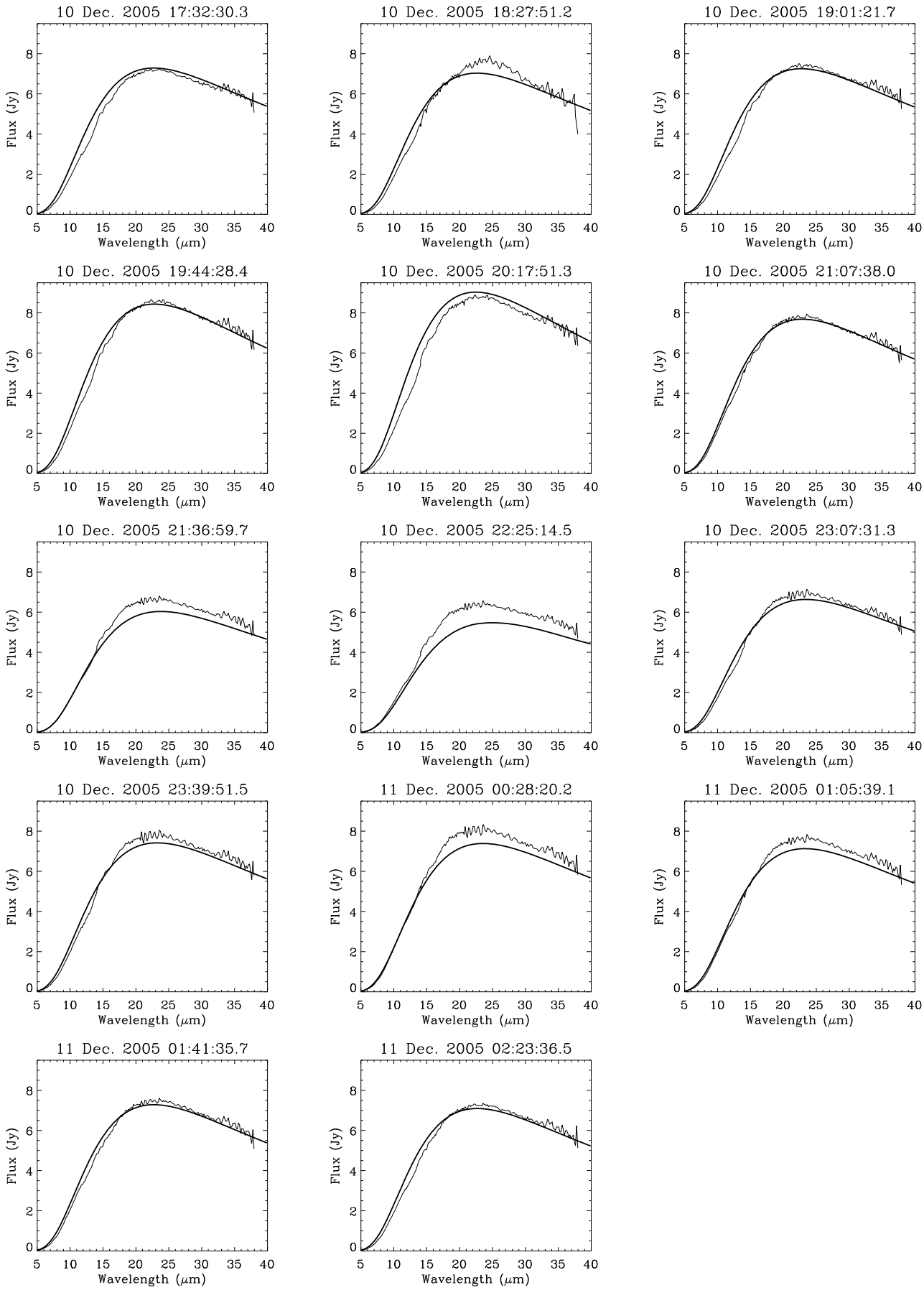

Fig. 1. The fourteen SEDs of Lutetia over the full spectral range 5–38 μm (thin lines). The thick solid lines correspond to the SEDs calculated with our model for the combination of thermal parameters $I = 0$ and $\eta = 0.83$ (see text for details).

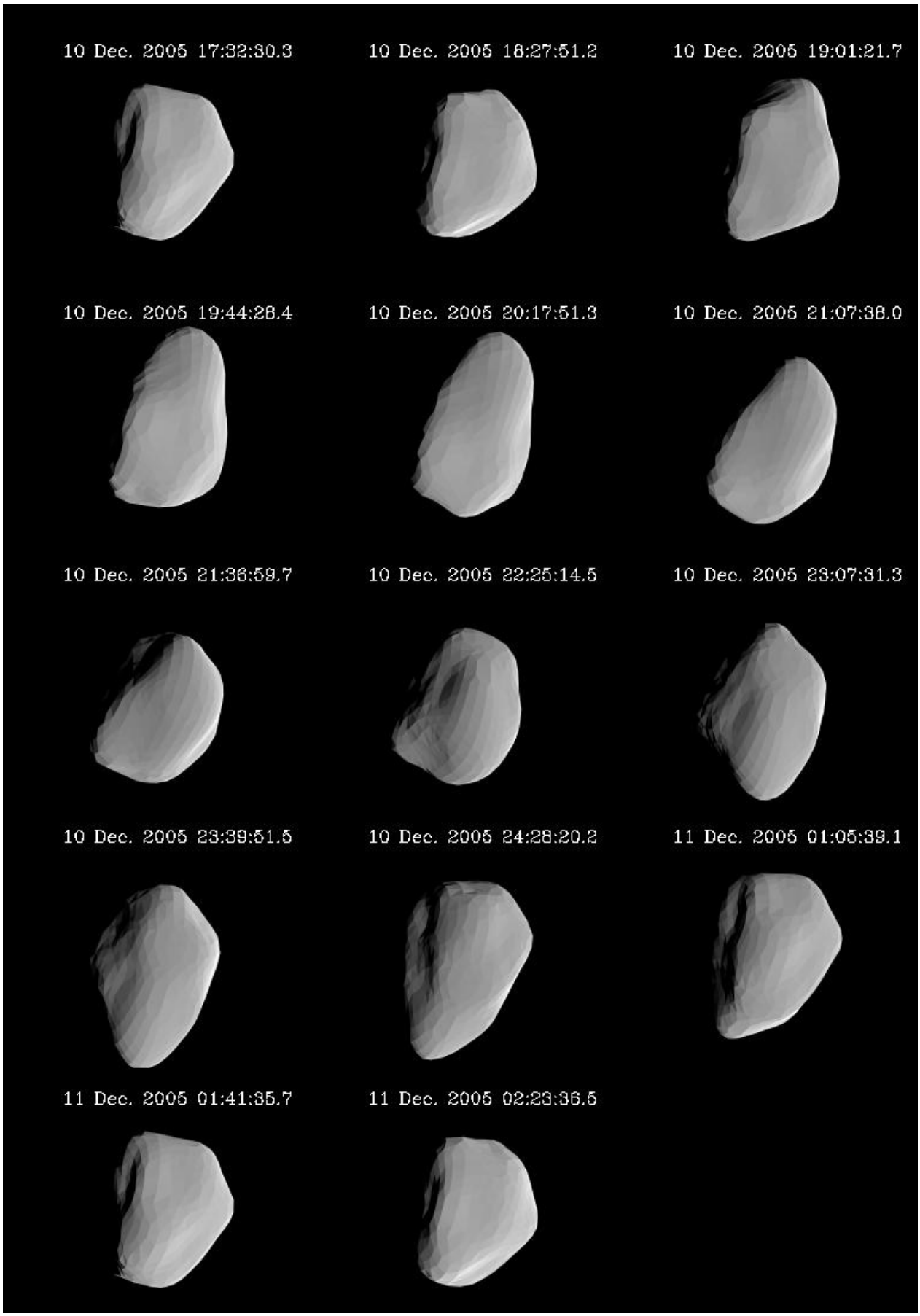

Fig. 2. Fourteen views of Lutetia as it would have appeared to the SST in the visible (i.e., reflected light) at the time of the 14 visits. The orientation is such that the aspect angle (defined as the angle between the spin vector and the asteroid-observer vector) equals 75°, close to an equatorial view.

we obtained the temperature of each facet as a function of time, over one period of rotation and then calculated the infrared flux F_i from each facet of index i as a function of time using Eq. (3):

$$F_i(\lambda) = \frac{\epsilon}{\Delta^2} B(\lambda, T_i) u_i \cos(w_i) \mathrm{d}S_i \quad (3)$$

where λ [μm] is the wavelength; Δ [km] the distance to the observer (SST in our case); B is the Planck function; u_i the view factor between facet i and the observer ($u_i = 1$ if the observer sees the facet; $u_i = 0$ otherwise); w_i the incident angle of the facet i; and $\mathrm{d}S_i$ the surface area of facet i. The total flux received by the observer is the sum of the individual fluxes F_i over all facets of the shape model. It is computed at different wavelengths λ to construct the spectral energy distribution.

The assumption of a constant Bond albedo implicit in Eq. (1) above is not strictly valid as it is generally a function of wavelength. Inspection of the spectra of Lutetia obtained in the visible (Barucci et al. 2005) and in the near infrared (Nedelcu et al. 2007) indicates a very modest spectral reddening up to 0.8 μm and a flat reflectance beyond. We can safely ignore this slight effect on the further ground that, when the reddening is much more pronounced as in the case of 2867 Steins, taking the spectral variation of the albedo into account has a negligible impact on the determination of the thermal parameters (Lamy et al. 2008).

3.3. Parameters of the thermal model

Our model has four free parameters: the infrared emissivity ϵ, the Bond albedo A_v, the beaming factor η, and the thermal inertia I.

The infrared emissivity ϵ is taken as equal to 0.95, the middle point of the interval 0.9–1.0 always quoted in the literature. As the interval is very small and the value near 1.0, this uncertainty has a negligible influence on the calculated thermal flux.

The Bond albedo A_v is the product of the visible geometric albedo p_v and of the phase integral q. We used $p_v = 0.13$, as derived by Lamy et al. (2010) from OSIRIS-Rosetta observations, using the same shape model as in this study and $q = 0.376$, derived from the relationship $q = 0.290 + 0.684G$ (Bowell et al. 1989) with $G = 0.125$ (Belskaya et al. 2010). Altogether, this gives $A_v = 0.049$.

The beaming factor η follows the strict definition given by Lagerros (1998), and therefore only reflects the influence of surface roughness. Theoretically η ranges from 0 (largest roughness) to 1 (flat surface), but in practice it must be larger than 0.7 to avoid unrealistic roughness, with rms slopes exceeding 45 deg (Lagerros 1998). In this study, η is unknown and derived from the observations.

The thermal inertia is also unknown, and we covered a range 0–50 $\mathrm{JK^{-1}m^{-2}s^{-1/2}}$ with six values $I = 0, 10, 20, 30, 40$ and 50 $\mathrm{JK^{-1}m^{-2}s^{-1/2}}$. As demonstrated later, higher values are not compatible with the observations.

Finally, there are only two unknown parameters in the thermal model, the thermal inertia I, and the beaming factor η. These two parameters have a similar effect as they change the surface temperature distribution. As such, they cannot be determined independently, and to each value of I corresponds one value of η.

4. The thermal properties of asteroid 21 Lutetia

The thermal properties were determined in two steps. First, we derived the thermal inertia I and roughness η from the thermal light curve, and then studied the implications for the individual SEDs presented in Fig. 1.

Table 2. Thermal inertia I and beaming factor η of asteroid 21 Lutetia derived from the SST data, for two different values of the geometric albedo.

	Nominal value $p_v = 0.13^\dagger$		Extreme value $p_v = 0.26^\ddagger$	
I ($\mathrm{JK^{-1}m^{-2}s^{-1/2}}$)	η^a	χ^2 ($\mathrm{Jy^2}$)	η^a	χ^2 ($\mathrm{Jy^2}$)
0	0.83 ± 0.05	69	0.78 ± 0.05	69
10	0.76 ± 0.05	79	0.72 ± 0.05	79
20	0.71 ± 0.05	83	0.67 ± 0.05	83
30	0.67 ± 0.05	84	0.63 ± 0.05	84
40	0.64 ± 0.05	83	0.60 ± 0.05	84
50	0.61 ± 0.05	82	0.57 ± 0.05	81

Notes. $^{(a)}$ The uncertainty of ±0.05 on η is obtained by doubling the χ^2 value.
References. †: Lamy et al. (2010); ‡: Mueller et al. (2006).

4.1. Thermal light curve

Using the above shape and thermal models, we generated synthetic thermal light curves of asteroid Lutetia as seen from the SST in December 2005. For each value of the thermal inertia in the range 0–50 $\mathrm{JK^{-1}m^{-2}s^{-1/2}}$, the best value for η was determined by a least-square fit of the synthetic light curve to the observed one. All light curves were calculated by integrating the respective SEDs from 5 to 37 μm. Their phasing is absolute in time since the rotation period is known with sufficient accuracy, better than 0.01 s. The results are presented in Table 2 and illustrated in Fig. 3 (upper panel).

As shown in Table 2, the beaming factor decreases as the thermal inertia increases. In fact, when I increases, more energy is used for internal heat conduction and less for surface heating (Eq. (1)), so that the surface temperature decreases overall. To match the observations and maintain a constant thermal flux from the surface, surface cooling must be compensated by a lower beaming factor (that is, a higher roughness), which in turn increases the surface temperature. As explained in Sect. 3.3, the beaming factor must be greater than 0.7 to avoid unrealistic roughness. This constraint $\eta > 0.7$ imposes that the only acceptable values of I must lie in the range 0–30 $\mathrm{JK^{-1}m^{-2}s^{-1/2}}$ for the nominal value of the geometric albedo $p_v = 0.13$ considered in Sect. 3.3. This constraint would restrict the above range to 0–20 $\mathrm{JK^{-1}m^{-2}s^{-1/2}}$ in the case of the extreme geometric albedo $p_v = 0.26$ derived by Mueller et al. (2006) using their thermophysical model (TPM). However, since the value $p_v = 0.13$ of Lamy et al. (2010) is based on more recent photometric observations analyzed with an up-to-date shape model, we favor the range 0–30 $\mathrm{JK^{-1}m^{-2}s^{-1/2}}$, which includes the high albedo case.

Figure 3 (upper panel) displays the synthetic thermal light curves of 21 Lutetia at the time of the SST observations, for the combinations ($I = 0$, $\eta = 0.83$) and ($I = 30$ $\mathrm{JK^{-1}m^{-2}s^{-1/2}}$, $\eta = 0.67$). Similar results were obtained for the other combinations of parameters presented in Table 2. Qualitatively, the results are impressive since the general shape of the light curve with two extrema (maximum at UT ~ 20.5 h and minimum at UT ~ 22.0 h) followed by a plateau (at UT ~ 24–27 h) is reproduced well in phase and, to a lesser extent, in intensity. Quantitatively, the synthetic curves match 8 out of the 14 SST data points at the 1σ level, and 12 of them at the 3σ level. The fit is, however, not perfect since the model gives a flux that is too large by ~8% close to the maximum, too low by ~16% close

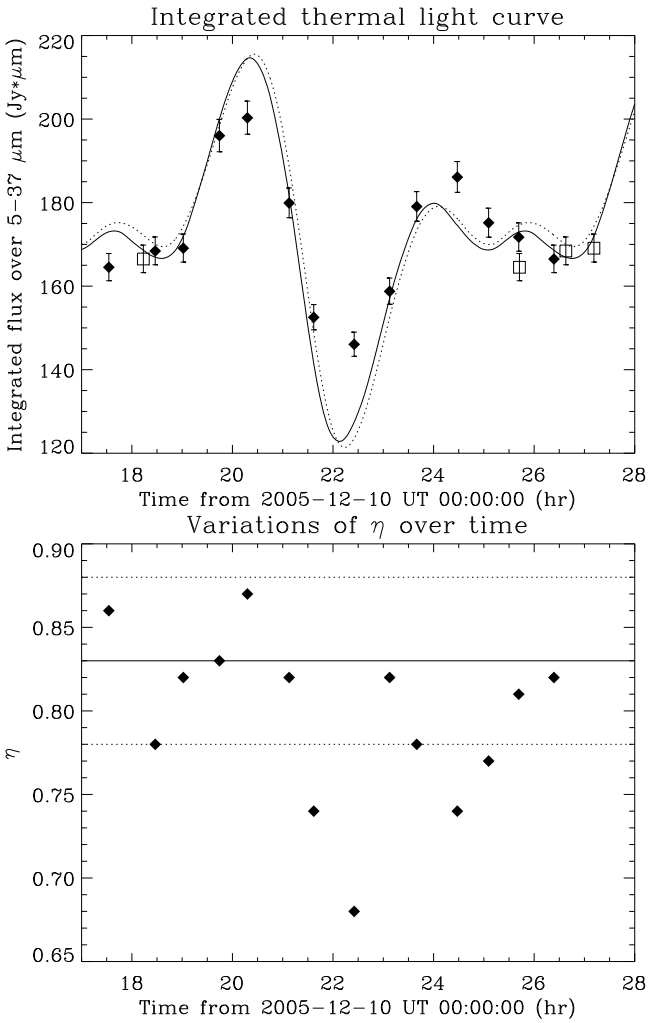

Fig. 3. *Upper panel*: Thermal light curves of asteroid 21 Lutetia. The symbols correspond to the SST observations (the open squares correspond to phased-folded data points). The solid line corresponds to the synthetic thermal light curve with the combination ($I = 0, \eta = 0.83$), while the dotted line corresponds to the combination ($I = 30$ JK^{-1}m^{-2}s$^{-1/2}$, $\eta = 0.67$). *Lower panel*: Variations in the η parameter with time for a constant thermal inertia $I = 0$ (see Sect. 4.2 for details). The horizontal solid and dashed lines correspond to the nominal value $\eta = 0.83 \pm 0.05$ for $I = 0$ given in Table 2.

to the minium, and too low by ∼4% close to the middle of the plateau. These discrepancies are discussed in the next section.

4.2. Spectral energy distributions

Figure 1 presents the fourteen SEDs of Lutetia over the full spectral range 5–38 μm, together with the synthetic SEDs from our thermal model for the combination $I = 0$ and $\eta = 0.83$. Since the thermal light curves presented in Fig. 3 (upper panel) were directly obtained by integrating the individual SEDs, we notice the same discrepancies in the absolute values of the flux at the extrema (UT ∼ 20:17 h and UT ∼ 22:25 h) and at the plateau (UT ∼ 00:28 h).

These discrepancies most likely result from errors in the shape model. In particular, the c (north/south) axis of the model is not well constrained, and that could affect the thermal light curve since Lutetia was viewed by the SST with a nearly equatorial aspect; any error on c directly translates to an error on the apparent cross-section and in turn on the thermal light curve. Projected shadows may furthermore play an important role in controlling the plateau (UT ≃ 24–27 h), as illustrated in Fig. 2. A slightly different local topography could decrease the projected shadows, and therefore increase the thermal flux of the asteroid to better match the data. This effect is particularly relevant for Lutetia, which has a low thermal inertia, and thus an almost instantaneous response of the surface temperature to insulation.

Another possible cause of the above discrepancies is variations in surface roughness. In Fig. 1, the value of η is assumed constant over the entire surface, but this may not be the case. Indeed, Nedelcu et al. (2007) and Busarev (2008), who observed Lutetia with a near equatorial aspect like we did, reported variations in the spectral slope of Lutetia with rotational phase in the visible and near-infrared domains.

These variations may stem from inhomogeneities in the surface roughness, and we quantified this effect by adjusting the η value of our model to fit each observed SED. The results are presented in Fig. 4 for a zero thermal inertia, which shows a drastic improvement compared to Fig. 1. η is then a function of rotational phase (Fig. 3, lower panel), with two regions clearly below the nominal range of 0.83 ± 0.05 given in Table 2, at times ∼22.5 h and ∼24.5 h. For these two particular regions, η drops to 0.68 and 0.74. According to Lagerros (1998), for a low albedo surface such as that of Lutetia, a change in roughness from $\eta = 0.87$ (highest value) to $\eta = 0.68$ (lowest value) corresponds to a variation in r.m.s slopes from ∼25° to ∼45°. With observed values for other asteroids in the range 0–40° and a mean value around 10° (Thomas et al. 2007), this is likely at the limit of what is physically acceptable. But since roughness variations and shape effects cannot be separated, the most plausible explanation is probably a combination of these two effects.

While the absolute value of a SED is determined by the size of the body, its shape is a diagnostic of the thermal properties (thermal inertia and roughness) of the surface. As we can see in Fig. 4, the shape of the SEDs is reproduced very well by the different combinations of $I = 0$ and η. We obtained similar results for the other valid combinations of I and η presented in Table 2. This further reinforces our conclusions of a thermal inertia in the range 0–30 JK^{-1}m^{-2}s$^{-1/2}$ and a beaming factor in the range ∼0.70–0.83.

Our result agrees with those of Mueller et al. (2006), $I = 0$–100 JK^{-1}m^{-2}s$^{-1/2}$, and Carvano et al. (2008), $I = 5.2^{+0.9}_{-0.3}$ JK^{-1}m^{-2}s$^{-1/2}$. This is also a typical range for large (>100 km) main-belt asteroids, as summarized by Delbó et al. (2009). This suggests that the surface of Lutetia is likely covered by a thick regolith layer, comparable to the Moon, whose thermal inertia was estimated to 43 JK^{-1}m^{-2}s$^{-1/2}$ by Wesselink (1948).

5. Implications for the Rosetta flyby of 21 Lutetia

The Rosetta spacecraft will fly by asteroid 21 Lutetia on 10 July 2010. Surface temperature measurements will be performed by the VIRTIS (Coradini et al. 1999) and MIRO (Gulkis et al. 2007) instruments. To facilitate the interpretation of these observations, we carried out a simulation of the flyby using the OASIS simulator (Jorda et al. 2010) and a more detailed shape model than is presented in Sect. 3.1. This refined model is composed of 131 072 facets. To make it more realistic, a random distribution of craters was added to the surface, and local topography was simulated using an algorithm that generates fractal terrains.

As illustrated in Fig. 5, we calculated the images that will be obtained by the ORISIS narrow angle camera (NAC) at different

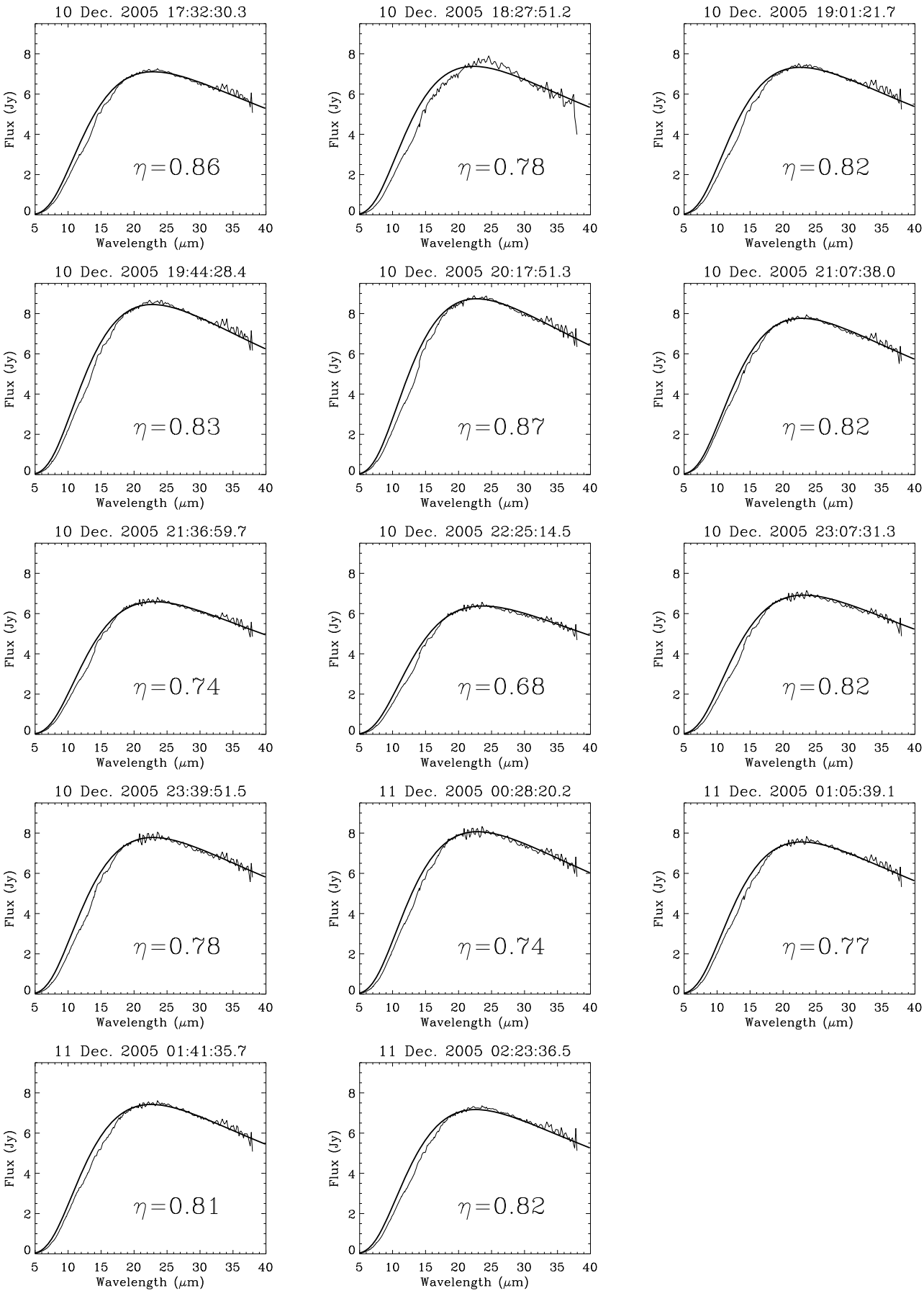

Fig. 4. The fourteen SEDs of Lutetia over the full spectral range 5–38 μm (thin lines). The thick solid lines correspond to the SEDs calculated with our model assuming a constant thermal inertia $I = 0$ and a variable value of η (see text for detail).

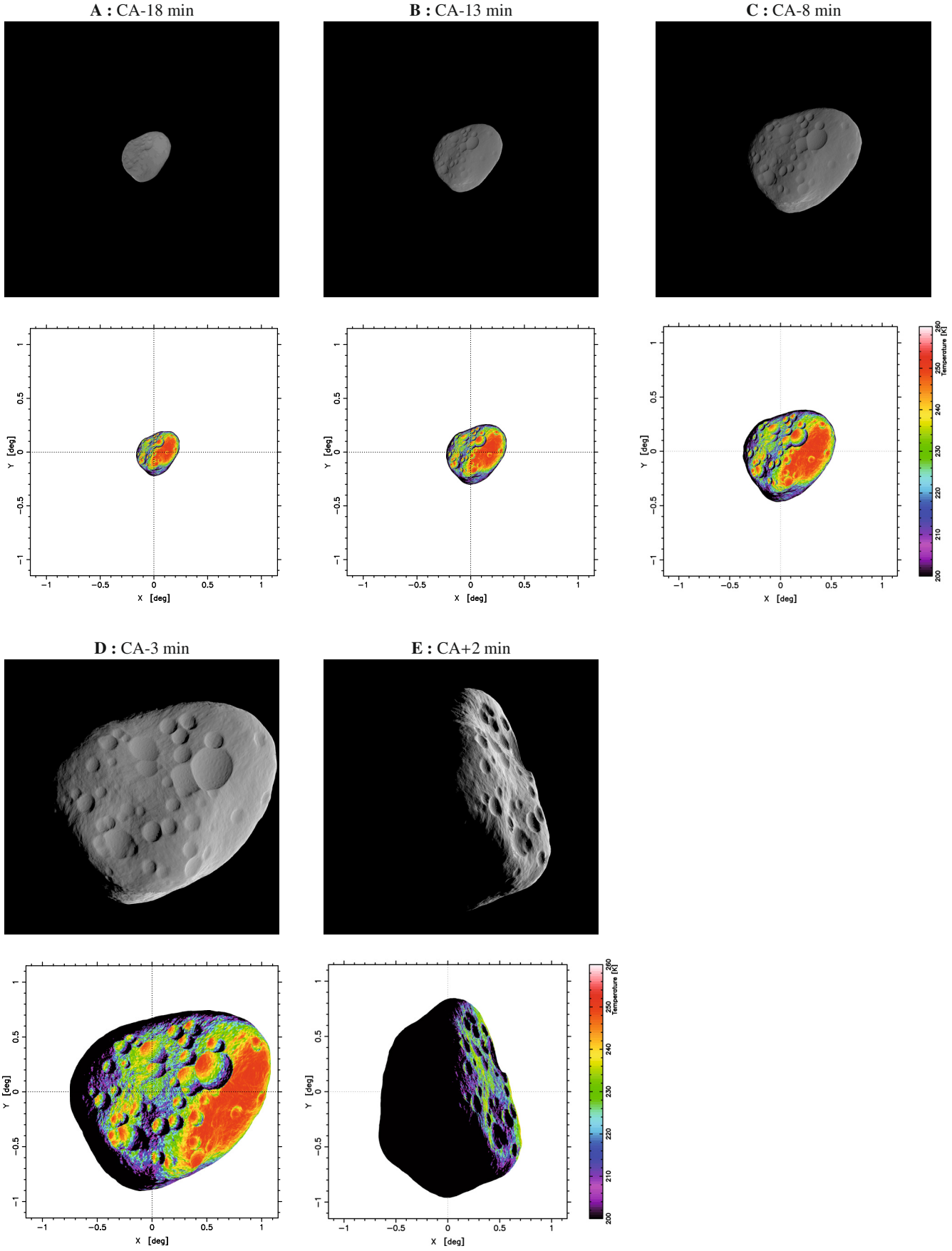

Fig. 5. Simulated visible (in black and white) and thermal (in color) images of asteroid 21 Lutetia during the forthcoming Rosetta flyby on 10 July 2010. Images were calculated at distances of 16 300 km (panel **A**), 11 800 km (panel **B**), 7600 km (panel **C**), 3900 km (panel **D**), and 3700 km (panel **E**) from the asteroid, corresponding to phase angles of 0°, 4°, 13°, 40°, and 110°, respectively. CA stands for Closest Approach (3055 km).

times during the flyby and the corresponding surface temperature maps for the combination of thermal parameters $I = 0$ and $\eta = 0.83$. During approach, the geometry is relatively constant and the aspect angle does not change significantly; surface temperatures vary between 200 K and 260 K on the illuminated side. The warmest region is located close to the subsolar point, but many hot spots (>250 K) are also visible at larger zenithal angles, mainly in craters where incident angles are small. After closest approach, at larger phase angles, hot spots facing the Sun are hidden by the local topography (crater rims), and we only see cold regions, most of them with temperatures below ≃230 K.

6. Conclusions

Our SST observations of asteroid 21 Lutetia, the second target of the Rosetta mission, have enabled us to ascertain its physical properties. Our main findings are summarized below.

1. The thermal inertia is in the range 0–30 $\mathrm{JK^{-1}m^{-2}s^{-1/2}}$. This value is consistent with the results of Mueller et al. (2006) and Carvano et al. (2008), and typical of large main belt asteroids (Delbó et al. 2009). This low thermal inertia implies that the surface of Lutetia is likely covered by a thick regolith layer, but it does not really constrain its composition (stony, metallic, or mixed) since it prominently results from voids in the (loose) regolith.
2. The upper limit of the thermal inertia of 30 $\mathrm{JK^{-1}m^{-2}s^{-1/2}}$ is, in fact, constrained by the lower limit imposed on the beaming factor $\eta \gtrsim 0.7$. For a zero thermal inertia as favored by our modeling, we obtained $\eta = 0.83 \pm 0.05$. Since our beaming factor only reflects the effects of surface rugosity (Lagerros 1998), the above result indicates that the surface roughness of Lutetia is larger than on other asteroids (Thomas et al. 2007), with an average slope over ∼25°.
3. There is evidence of inhomogeneities in the surface roughness in the equatorial band of Lutetia with two particular regions where η drops to 0.68 and 0.74, the lowest value implying slopes up to ∼45°.
4. To first order, the current shape model of Lutetia provides a good fit to the thermal light curve, indicating that it is already quite accurate.
5. However, small discrepancies between the synthetic and observed thermal light curves could result from shape uncertainties on the c axis (north/south direction), projected shadows due to local topographic uncertainties, and roughness inhomogeneities as mentioned above.

Acknowledgements. This work is based on observations made with the *Spitzer* Space Telescope, which is operated by the Jet Propulsion Laboratory, California Institute of Technology under a contract with NASA. We thank the SST ground system personnel for their prompt and efficient scheduling of the observations. We are grateful to I. Belskaya for making her results available to us in advance of publication.

References

Barucci, M. A., Fulchignoni, M., Fornasier, et al. 2005, A&A, 430, 313
Belskaya, I. N., Fornasier, S., Krugly, Y. N., et al. 2010, A&A, 515, A29
Bowell, E., Hapke, B., Domingue, D., et al. 1989, In Asteroids II, ed. R. P. Binzel, T. Gehrels, & M. S. Matthews (Tucson: Univ. of Arizona Press), 524
Busarev, V. V. 2008, ACM conference, abstract 8010
Carry, B., Kaasalainen, M., Leyrat, C., et al. 2010, A&A, submitted
Carvano, J. M., Barucci, M. A., Delbó, M., et al. 2008, A&A, 479, 241
Coradini, A., Capaccioni, F., Drossart, P., et al. 1999, Adv. Space Res., 24, 1095
Delbó, M., & Tanga, P. 2009, Planet Space Sci., 57, 259
Drummond, J., D., Conrad, A., Merline, W., & Carry, B. 2009, DPS meeting 41, 59.07
Groussin, O. Lamy, P., & Jorda, L. 2004, A&A, 413, 1163
Gulkis, S., Frerking, M., Crovisier, et al. 2007, Space Sci. Rev., 128, 561
Houck, J. R., Roellig, T. L., van Cleve, J., et al. 2004, ApJS, 154, 18
Jorda, L., Spjuth, S., Keller, H. U., Lamy, P., & Llebaria, A. 2010, SPIE, submitted
Keller, H. U., Barbieri, C., Koschny, D., et al. 2010, Science, 327, 190
Lagerros, J. S. V. 1996, A&A, 310, 1011
Lagerros, J. S. V. 1998, A&A, 332, 1123
Lamy, P., Jorda, L., Fornasier, S., et al. 2008, A&A, 487, 1187
Lamy, P., Faury, G., Jorda, L., Kassalainen, M., & Hviid, S. F. 2010, A&A, accepted
Mueller, M., Harris, A. W., Bus, S. J., et al. 2006, A&A, 447, 1153
Nedelcu, D. A., Birlan, M., Vernazza, P., et al. 2007, A&A, 470, 1157
Tedesco, E. F., Veeder, G. J., Fowler, J. W., & Chillemi, J. R. 1992, in The IRAS Minor planet Survey, Tech. Rep. PL-TR-92-2049, Phillips Laboratory, Hanscom Air Force Base, Massachusetts
Thomas, P. C., Veverka, J., Belton, M. J. S., et al. 2007, Icarus, 187, 4
Torppa, J., Kaasalainen, M., Michalowski, T., et al. 2006, Icarus, 164, 346
Weaver, H. A., Feldman, P. D., Merline, W. J., et al. 2010, A&A, accepted
Werner, M. W., Roellig, T. L., & Low, F. J. 2004, ApJS, 154, 1
Wesselink, A. J. 1948, Bull. Astron. Inst. Neth., 10, 351